Featured in Physics

Raman Wavelength Conversion in Ionic Liquids

Rotem Kupfer,[1,*,§] Furong Wang,[2,†] James F. Wishart,[2,‡] Marcus Babzien,[1] Mikhail N. Polyanskiy,[1] Igor V. Pogorelsky,[1] Triveni Rao,[3] Luca Cultrera,[3] Navid Vafaei-Najafabadi,[1,4] and Mark A. Palmer[1]

[1] *Accelerator Test Facility, Brookhaven National Laboratory, Upton, New York 11973 USA*
[2] *Chemistry Division, Brookhaven National Laboratory, Upton, New York 11973 USA*
[3] *Instrumentation Division, Brookhaven National Laboratory, Upton, New York 11973 USA*
[4] *Department of Physics and Astronomy, Stony Brook University, Stony Brook, New York 11794, USA*

(Received 16 June 2022; accepted 8 December 2022; published 19 January 2023)

We explore the use of room-temperature ionic liquids (ILs) as Raman wavelength converters. ILs provide an engineerable framework to design suitable liquids for wavelength conversion over a broad spectral range, through careful selection of the molecular structures of the IL anions and cations so that specific characteristics can be obtained, such as a desirable Raman shift, low Brillouin scattering, and good optical transmission in the pump and Stokes wavelengths. Applying such criteria, we demonstrate that 1-ethyl-3-methylimidazolium dicyanamide (EMIM DCA) is an effective medium for conversion of 532-nm pulses from a Q-switched Nd :YAG laser to 603 nm. This corresponds to an approximate 2200 cm^{-1} shift, which can be used to generate mid-infrared radiation through subsequent difference frequency generation for optical pumping of CO_2 lasers. Threefold-higher Raman conversion efficiency is obtained in EMIM DCA compared with water under identical conditions in a proof-of-principle single-pass conversion setup, resulting in an efficient generation of multimillijoule, <6 ns duration, high-quality orange laser pulses in a wavelength region that is difficult to access at high energies. Consequently, we examine ILs representing two other classes of Raman-active functional groups and obtain conversion up to the fifth-order Stokes shift and first anti-Stokes shift. Through the tunable selection of their components and their useful dynamical properties, ILs provide a platform for efficient, simple, and alignment-tolerant high-energy Raman shifting with numerous industrial and technological applications.

DOI: 10.1103/PhysRevApplied.19.014052

I. INTRODUCTION

Efficient, high energy (> a few millijoules), short pulse (about a few nanosecond, picosecond, or femtosecond scale) laser sources only exist in a limited number of wavelengths. If an application requires a wavelength that cannot be produced directly from a laser, a wavelength conversion method is needed, typically in the form of a nonlinear optical process [1], and even then, some spectral regions are not easily accessible. One example of such a region is the yellow-orange spectral range (570–625 nm) that is of particular interest for medical applications [2] in dermatology [3,4], ophthalmology [5], and flow cytometry [6], among others. In addition, if one could obtain an efficient pulsed orange laser source, coherent mid-infrared (MIR) radiation for optical pumping of CO_2 lasers could be generated through difference frequency generation (DFG) from green light. For these reasons, finding new techniques to convert light from existing laser sources into this spectral range is appealing.

Stimulated Raman scattering (SRS) [1,7] is an efficient method of obtaining high-energy laser pulses at wavelengths that are otherwise hard to generate, by wavelength shifting of an available pump source in a Raman-active medium. SRS is stimulated inelastic scattering of photons from a coherently excited state of the system, and it can be achieved in any state of matter, including solids, liquids, and gases [8]. In molecular SRS, the pump wavelength is converted into Stokes and anti-Stokes wavelengths that are shifted by the dominant bond vibration frequency, $\omega_R = \omega_L \pm N_R\omega_v$, where $\omega_L, \omega_R, \omega_v$ are the pump, Raman shifted and vibration frequencies, respectively, and N_R is the shift order in case of a cascade process. In other words, the shifts are defined by the molecular normal vibration modes, which are determined by the chemical and isotopic structure of the molecule.

*kupfer2@llnl.gov
†fwang1@bnl.gov
‡wishart@bnl.gov
§Current address: Lawrence Livermore National Laboratory, Livermore CA 94550, USA

While it may appear simple at first, the process of SRS in molecules is rather complex and different models and assumptions can capture different aspects of it. A comprehensive review can be found in Ref. [9]; the essentials are discussed next. By considering the effective Hamiltonian of an ensemble of molecules with a vibrational degree of freedom interacting with a nonresonant laser electric field and performing a steady-state second-quantized analysis considering only the first mode ($N_R = 1, \omega_R = \omega_S = \omega_L - \omega_v$), we can derive the Stokes photon generation rate,

$$\frac{dn_S}{dt} = N\left(\frac{\partial\alpha}{\partial q}\right)^2 \frac{4\pi^3}{\mu_L\mu_S^2 mc} I_L \sum_{k_S} \frac{\omega_S}{\omega_v} (\vec{\mathbf{e}_L} \cdot \vec{\mathbf{e}_S})^2 \times (1 + n_S + n_v)\delta(\omega_S - \omega_L + \omega_v), \quad (1)$$

where N is the number density of molecules in volume V; $\partial\alpha/\partial q$ is the normal-mode derivative of the molecular polarizability tensor with q being the normal mode amplitude and m the reduced mass; μ_L and μ_S are the permeabilities at the pump and Stokes wavelength, respectively; $I_L = (\hbar\omega_L c/\mu_L V)\ \Sigma_{k_L} n_L$ is the pump laser intensity; $\vec{\mathbf{e}_L}, \vec{\mathbf{e}_S}$ are the linear polarization vectors of the pump and Stokes, respectively; n_L,n_S,andn_v are the occupation numbers of the pump, Stokes, and molecular vibration modes; the summations are over all the laser (k_L) and Stokes (k_S) modes, c is the speed of light, $\hbar$ is the reduced Planck's constant, and δ is Kronker's delta. From the middle parentheses, we can see the contributions of spontaneous emission, stimulated emission, and parametric coupling of the Stokes light and material excitation, respectively. However, for moderate pumping, the contribution of n_v is generally negligible and its population is on the order of its thermal equilibrium value $n_v \sim (\exp(\hbar\omega_v/kT) - 1)^{-1}$, where k and T, are Boltzmann's constant and temperature, respectively. This is also the reason for the typical lower intensity of the anti-Stokes emission compared to Stokes, as most of the molecules are in the vibrational ground state at room temperature. The vector product in Eq. (1) is responsible for the polarization of the Stokes being generally the same as that of the pump. Furthermore, we can define the differential cross section for the spontaneous Raman ($n_S, n_v \approx 0$, assuming $\vec{\mathbf{e}_L} \cdot \vec{\mathbf{e}_S} = 1$),

$$\frac{\partial\sigma}{\partial\Omega} = \left(\frac{\partial\alpha}{\partial q}\right)^2 \frac{\omega_S^4\mu_S}{c^4\mu_L} \frac{\hbar}{2m\omega_v}, \quad (2)$$

and by assuming a narrow laser line and homogeneous broadening of the molecular transition, we can derive the Raman gain for the stimulated case,

$$g(\omega_S) = N\left(\frac{\partial\alpha}{\partial q}\right)^2 \frac{4\pi^2\omega_S}{\mu_L\mu_S c^2 m\omega_v} \frac{\Gamma}{(\omega_S - \omega_L + \omega_v)^2 + \Gamma^2}, \quad (3)$$

where $\Gamma = 1/T_2$ is the linewidth associated with the dephasing time (T_2, not to be mistaken with the excited state lifetime T_1) of the system. It should be noted that in most cases the driving laser field frequency is far from resonance with the electronic states of the molecule, so $\partial\alpha/\partial q$ can be treated as a constant. Another notable feature is the asymmetry between backward and forward SRS, favoring the latter, and that is mainly because of asymmetry in the Doppler line broadening [10]. While the full quantum mechanical approach shows the origin of SRS and its buildup from spontaneous noise, it is only valid in the steady state and the occupation number formalism does not provide any information on the phases. Phase information can be obtained from semiclassical analysis of the density matrix evolution by solving the Liouville equation. We also note that for the three-dimensional case, spatiotemporal effects play a major role, and current models have not fully reproduced the Stokes buildup profile that has been observed in experiments (see, for example, the supplemental material of Ref. [11]).

In the short-pulse regime, high conversion efficiency can be achieved with a pump-pulse duration that is longer than the vibration dephasing time (typically on the order of a few picoseconds) and a multipass [12] or cavity [13,14] configuration can be used to increase the interaction length. Of particular interest is the fact that any chirp in the pump pulse is maintained in the Raman-shifted pulses [15,16], so broadband, temporally stretched pump pulses can be used and the output pulses can be compressed later to ultrafast durations. In this application, chirped pump pulses from a conventional chirped pulse amplification system can be wavelength shifted and subsequently recompressed in a standard compressor to provide a temporally synchronized, spectrally distinct source that can be used as a probe, seed, or beat-wave generator for two-color laser-plasma experiments. For example, a detuned probe can be useful for high-energy-density physics experiments with solid targets that produce significant sub or high harmonics of the pump light.

Notable practical challenges in SRS conversion include forward and backward SRS, high-order Stokes and anti-Stokes generation, self-focusing and de-focusing, transient effects, stimulated Brillouin scattering (SBS), optical breakdown, and self-phase modulation, so the physical and thermal properties of the medium play a crucial role in the overall achievable conversion efficiency in addition to the inherent Raman gain.

Solids offer high densities of Raman active centers, high damage thresholds, and allow shorter interaction lengths, while the shift frequency is determined by the characteristic phonon frequencies and may depend on crystal orientation [8,14–19]. Typical shift frequencies are in the range of around 700–1300 cm^{-1} and conversion efficiencies of >70% have been observed. However, design and fabrication of large crystals for particular shift frequencies

is complex and expensive. In comparison, SRS in gases can provide higher-frequency shifts [17], for example, 4155 cm^{-1} in H_2, due to scattering from higher-frequency single-molecule vibrations, but the lower densities reduce the conversion efficiency, even at high pressure. Gas-filled hollow-core fibers [18–22] have been used to extend the interaction length to achieve high power in continuous wave operation, lower the SRS energy threshold at pulsed operation, and achieve overall higher efficiency. Gases also present higher thresholds for self-focusing and lower scattering losses compared with solids or liquids.

Liquids offer somewhat of a midway regime, with a higher density of Raman scattering centers compared to gases while still maintaining the single-molecule Raman shift. Ganot *et al.* [11] reported up to 35% conversion efficiency from 532 to 649 nm (approximately 3400 cm^{-1}) in liquid water, limited mostly due to thermal effects, absorption, and competing Brillouin scattering [11,23,24]. Self-guiding in filaments was shown to increase efficiency to around 60% [25] while even higher efficiency, 80%, was obtained in liquid molecular nitrogen [26]. By using aqueous sodium nitrate solution, Raman shifts to 564 and 599 nm were observed due to first- and second-order Stokes shifts from the nitrate ions [27]. In this case, the higher Raman cross section of the nitrate ion outcompeted the solvent water. Welch *et al.* [28], described a two-step scheme, Raman followed by DFG, that was used to generate long-wavelength infrared (LWIR) pulses. Deuterated benzene was used as a Raman medium to convert 1064-nm pulses from a mode-locked Nd:YAG laser to 1180 nm. The residual pump and the generated Stokes were then frequency-differentiated in a nonlinear GaSe crystal to generate 10.6-μm pulses, which correspond to a Raman shift of 944 cm^{-1}. However, efficiency was low because the pump laser duration was on the order of the Raman dephasing time.

Here, we propose the use of room-temperature ionic liquids (ILs), synthetic salts that are liquid at ambient temperature, as Raman wavelength converters. These liquids can be "designed" to have a given set of properties because they can be prepared in an infinite variety of combinations. While the use of ILs as solvents [29,30], electrolytes [27,31], lubricants [32–34], and in many other applications [35–37] has been extensively explored for years, there is no substantial prior work about their applicability as nonlinear optical materials. Many ILs have wide optical transmission windows and they are typically chemically stable. The viscosities of ILs are higher than most molecular liquids, helping to suppress the buildup of competing Brillouin scattering since the Brillouin gain [38–40], $g_B = \gamma^2/(n_P^3 c v_s \eta)$ scales inversely with viscosity, η, and n_p, v_s and γ are the refractive index at the pump wavelength, speed of sound in the medium and the electrostrictive coefficient, respectively. In particular, the specific structure of the liquid can be chosen in a way to provide a desired Raman shift with transparency at the pump and Stokes wavelengths.

II. RESULTS AND DISCUSSION

A. Tailoring an ionic liquid for a specific Raman wavelength shift

In this work, we focus on finding a suitable liquid for spectral shifting of the second harmonic (532 nm) of a *Q*-switched Nd:YAG laser by around 2200 cm^{-1}. This shift corresponds roughly to a 4.5-μm photon that can be generated down the line by DFG of the Stokes and residual pump and can be used for optical pumping of high-pressure mixed isotope CO_2 lasers [41–43] by directly exciting the upper laser level via the broadband vibrational transition $00^00 \rightarrow 00^01$ centered at 4.3 μm. Optical pumping is expected to enable the operation of CO_2 laser amplifiers at very high pressures (>10 bar) and high CO_2 concentrations (>10%). Such an operation regime, not achievable with gas-discharge pumping, is beneficial for (sub)picosecond LWIR laser systems [41,44,45]. Some detuning from this frequency (around 2325 cm^{-1}) is needed to better manage the absorption in the CO_2, so either lower or higher shifts within the bandwidth of this transition are preferable. For that goal, the selection process is as follows: (1) The liquid needs to have a dominant peak in the Raman spectrum around 2200 cm^{-1}. (2) The liquid should have good transmission in the pump and Stokes wavelengths, i.e., 532 nm and around 600 nm for Nd:YAG second-harmonic pumping, or 1064 nm and around 1390 nm for Nd:YAG fundamental pumping. In addition, the liquid should be chemically stable, have high enough viscosity to suppress Brillouin scattering, and have a low thermo-optical coefficient to minimize thermal effects.

We begin by seeking ILs with the desired Raman shift of about 2200 cm^{-1}. Raman spectra are acquired with a confocal Raman microscope (Witec Alpha) equipped with a 532-nm excitation laser. A single drop of a sample liquid is placed on a microscope slide and covered with a slip. Selected Raman spectra are presented in Fig. 1(a). The desired Raman characteristics can be designed into the IL by using anions containing nitrile groups (C—N triple bonds) that have intense Raman bands in the region of 2190–2230 cm^{-1}. Examples include the dicyanamide (DCA, $[N(CN)_2]^-$), tricyanomethanide (TCM, $[C(CN)_3]^-$), and tetracyanoborate (TCB, $[B(CN)_4]^-$) anions.

The next important criterion is high optical transmission at the pump and shift wavelengths, in this case based on the Nd:YAG fundamental and second harmonic, 1064 and 532 nm. Transmission spectra of representative ILs, measured using a PerkinElmer Lambda 950 UV-to-visible-to-near-infrared (UV-vis-NIR) spectrophotometer,

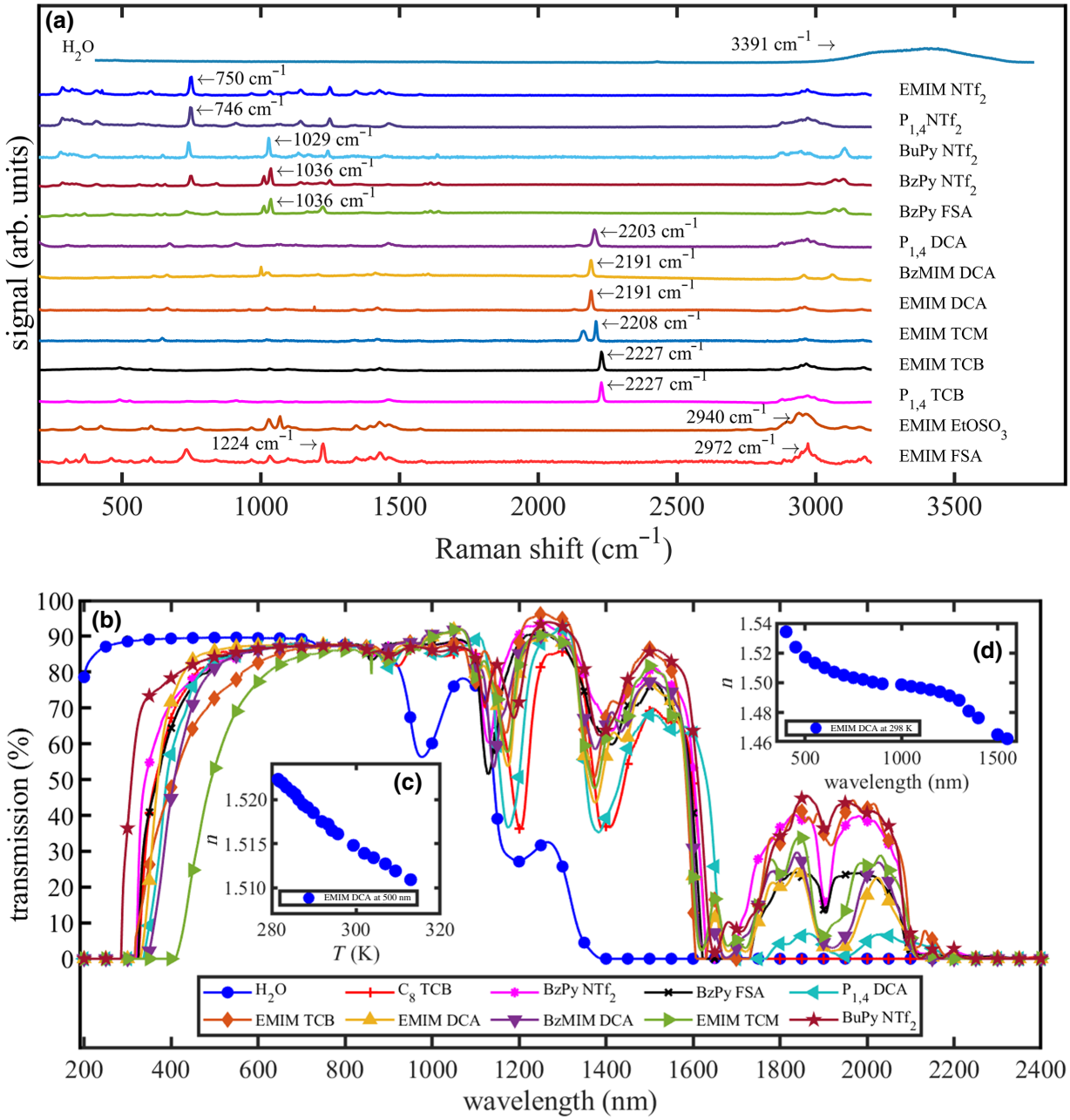

FIG. 1. Spectroscopic measurements of various ionic liquids. (a) Spontaneous Raman spectra of the surveyed ILs. The dominant Raman peak for each liquid is marked with an arrow. (b) Transmission spectra of various ILs showing extended transmission into the infrared compared with water. Note that the spectra are not corrected for Fresnel losses. (The sample of EMIM TCM used contains a colored contaminant that is responsible for the lower transmittance in the UV, but the focus is on the NIR.) (c) Refractive index of EMIM DCA as a function of wavelength at 298 K, (d) refractive index of EMIM DCA at 500 nm as a function of temperature. Abbreviations: (1) Cations: EMIM, 1-ethyl-3-methylimidazolium; $P_{1,4}$, 1-butyl-1-methylpyrrolidinium; BzMIM, 1-benzyl-3-methylimidazolium; BzPy, 1-benzylpyridinium; (2) Anions: NTf_2, bis(trifluoromethylsulfonyl)amide; FSA, bis(fluorosulfonyl)amide; DCA, dicyanamide; TCM, tricyanomethanide; TCB, tetracyanoborate; $EtOSO_3$, ethylsulfate. The ILs reported here are all used as received or synthesized. $P_{1,4}$ NTf_2, $P_{1,4}$ DCA, BzMIM DCA, EMIM DCA, and EMIM TCM purchased from IoLiTec (Ionic Liquids Technologies GmbH, Heilbronn, Germany). EMIM TCB and $P_{1,4}$ TCB purchased from EMD Chemicals. EMIM $EtOSO_3$ is a commercial sample from Solvent Innovations. EMIM NTf_2 [46], BzPy FSA, BzPy NTf_2 [47], and EMIM FSA [48] prepared in our laboratory.

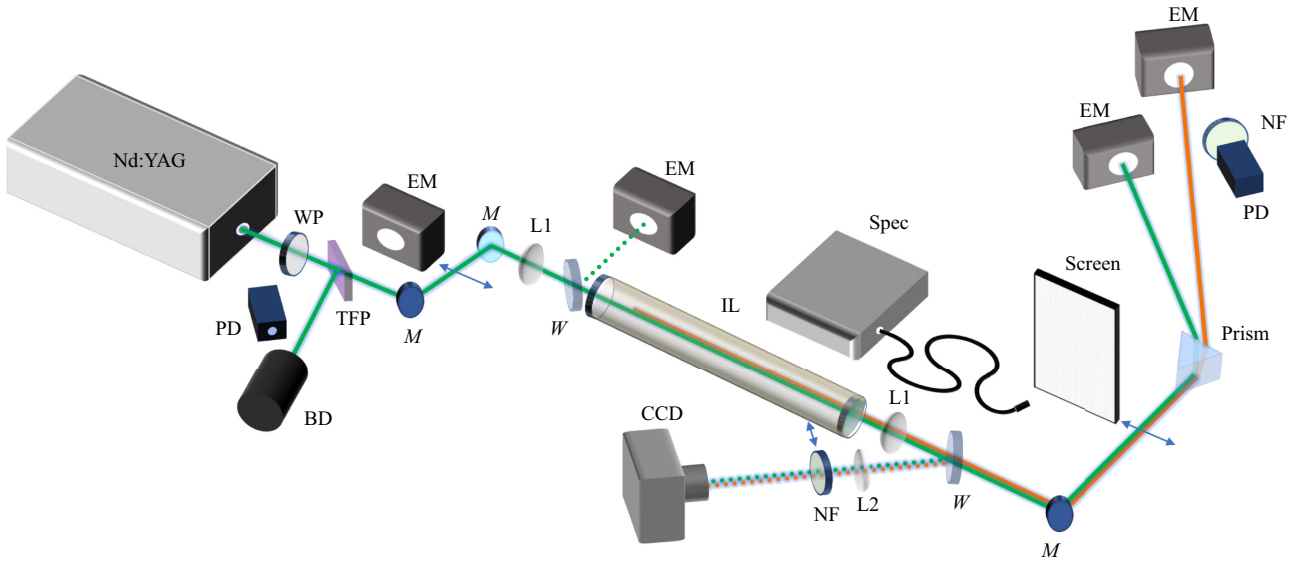

FIG. 2. Illustration of the experimental setup: The pump source is a frequency doubled Nd:YAG laser at 532 nm. We regulate a *p*-polarized transmitted pump energy by a $\lambda/2$ wave plate (WP) and a thin-film polarizer (TFP) while a reflected *s*-polarized component is sent to a beam dump (BD). The input pulse shape and energy are monitored with a fast photodiode (PD) and an energy meter (EM). The pump is focused and recollimated using a pair of 50-cm focal length lenses (L1). Back reflection and scattering are monitored using a wedged fused silica window (*W*) and an energy meter. Within the telescope, the pump passes through a 63-cm-long stainless-steel cell capped with 5-mm-thick sapphire windows and filled with EMIM DCA (IL). At the cell's output, we observe the profile of the pump or Stokes beam using the reflection from a wedge (*W*) that is focused to a CCD camera using a 15-cm focal length lens (L2) through a removable notch filter (NF). The pump and Stokes beams are separated by an equilateral prism and sent to two energy meters. The Stokes temporal profile is monitored by a second fast photodiode equipped with a notch filter. The spectrum after the cell is acquired using a fiber-coupled spectrometer (Spec) with the fiber tip pointing to a screen that is inserted into the beam path. Turning mirrors are labeled with *M*.

are shown in Fig. 1(b). While the ILs generally have clear transmission windows at 532 nm and its Stokes-shift region, shifts derived from 1064 nm may fall into a region where the IL absorbs. Absorption in the region around 1400 nm is primarily due to overtones of C—H stretching bands in the aliphatic regions of the cations. To minimize that absorption, the best IL cations for shifting 1064 nm would be those with the smallest numbers of aliphatic C—H bonds. Examples are aromatic (imidazolium or pyridinium) cations with the shortest aliphatic side chains that still form room-temperature ILs (e.g., 1-ethyl-3-methylimidazolium, or EMIM) or have aromatic side chains (e.g., 1-benzylpyridinium, or BzPy) since aromatic C—H bond overtones absorb in another, less important region. Based on the optical transmission and Raman spectra, we pick EMIM DCA as the first candidate for the wavelength conversion studies.

For a complete description of the relevant optical properties, we also measure the refractive index of EMIM DCA, both as a function of wavelength and temperature, as presented in Figs. 1(c) and 1(d), respectively. Refractive indices are measured using an Atago DR-M2 1550 refractometer equipped with an infrared viewer, a thermoelectrically driven liquid chiller/heater for sample temperature control, and a set of bandpass filters. The refractive index exhibits an inflection point around 1200 nm, consistent with the absorption peak at that region. This can be understood directly from the Kramers-Kronig relations that relate the real and imaginary components of the refractive index. In particular, this variation is important when operating with pump and Stokes wavelengths that are close to and on opposing sides of an absorption peak, a situation that is unusual in nonlinear optics but possible with ILs. It is worth noting that the extended optical transmission windows of ILs could be used for refractive-index-matched cooling of laser gain media [49] in the NIR region, in particular, when considering their good thermal conductivity and heat capacity [50–52]. From the temperature dependence of the refractive index, we deduce the thermo-optical coefficient to be around -3.5×10^{-4} K^{-1}, which is conveniently negative for our purposes and comparable in magnitude to that of liquid water.

B. High-energy wavelength conversion

To evaluate the applicability of ILs as Raman converters at high energies, we assemble a simple convertor setup and compare the performance of EMIM DCA versus liquid water under identical conditions. The setup is depicted

in Fig. 2. We use 532-nm, 9.8-ns laser pulses, with energies up to 115 mJ, from a frequency-doubled Nd:YAG laser at 12 Hz repetition rate. We adjust the input energy using a $\lambda/2$ wave plate and a thin-film polarizer to keep other laser parameters such as beam profile and pulse duration identical during energy scans. The p-polarized pump beam is focused using a 50-cm lens and sent for a single pass through a 63-cm-long cell filled with liquid (water or EMIM DCA) and capped with 5-mm-thick sapphire windows. Our experimental conditions are below the threshold for optical breakdown in both liquids. Back reflection and Brillouin scattering are monitored by a wedged fused-silica pickoff window and an energy meter. After recollimation using a second 50-cm lens, we image the reflection off a second wedge pickoff using a CCD camera and a removable notch filter to observe the pump and Stokes beam profiles. An equilateral prism is used to separate the pump and Stokes beams, and each beam is measured using a dedicated energy meter. The pump and Stokes temporal profiles are recorded using two fast photodiodes (2-GHz bandwidth) and an oscilloscope (500-MHz bandwidth), and the spectra are obtained using a fiber-coupled spectrometer (Ocean Insight FLAME-S-XR1-ES).

The conversion efficiencies from pump to first Stokes as a function of pump-pulse energy for water and EMIM DCA are presented in Fig. 3(a). This efficiency is defined as $E_{\mathrm{Stokes}}/(\beta E_{\mathrm{pump}})$, where $E_{\mathrm{pump}}, E_{\mathrm{Stokes}}$, and β are the pump-pulse input energy, Stokes pulse energy, and the optical transmission of the setup without liquid, as measured with an empty cell. The energies are recorded after thermal stabilization, which occurs after around 10 sec from the moment of turning the pump on, and averaged over 120 shots. It should be noted that Raman output actually drops during this thermal stabilization from an initial approximately 30% higher value. EMIM DCA shows a lower pump threshold for the initiation of Raman conversion and noticeably higher efficiency, up to around 38%. It also proves to be resistant and pure enough to avoid electrical breakdown and plasma generation, and no discoloration or deterioration is observed after the experiment. Brillouin back-scattering efficiencies, defined as the excess back-reflected signal on top of reflection from the optics, are shown in Fig. 3(b). As expected, the higher viscosity of EMIM DCA, 14.5 mPa s at 25 °C [53], results in a negligible Brillouin signal.

We observe the spectrum of the emitted light after the IL converter by pointing the tip of the spectrometer's collection fiber at a screen that is placed in the path of the beams. The measured spectra are shown in Fig. 3(c). Note that the relative intensities of the peaks depend on the orientation of the collection tip and do not represent the actual relative intensities, which are accurately measured with energy meters. For water, we observe the expected first Stokes peak at 652 nm, corresponding to a Raman shift of 3460 cm^{-1}, while EMIM DCA shows both first- and second-order Stokes peaks at 603 and 695 nm, corresponding to a Raman shift of 2200 cm^{-1}. This implies a higher Raman cross section for EMIM DCA compared with water. Nevertheless, the actual energy at the second Stokes peak is lower than the measurement threshold of our energy meters. In addition, if conversion to the next order becomes a limiting factor, one could conceivably mix in a small concentration of a solute having absorption around the second Stokes frequency to prevent its buildup.

The oscilloscope traces of the pump and Stokes pulses are presented in Fig 3(d). As expected, due to the nonlinear process, the Stokes pulse is shortened by 40% compared with the pump, 5.9 ns compared with 9.8 ns. Similarly, the beam profile of the Stokes beam also shows improvement over the pump, as can be seen in Figs. 3(e) and 3(f). It appears that the nonlinear process effectively conditions the multimode structure of the pump, resulting in a noticeably narrower beam that is closer to a single-mode profile.

Finally, to evaluate the durability of EMIM DCA in this application, we compare a postexperiment sample of the liquid with an unused one. We are looking for evidence of any breakdown- or heat-induced decomposition products [46,54,55]. However, the before-and-after UV-vis (taken with an Agilent Cary 60 spectrometer) and fluorescence spectra (measured with a Horiba Fluorlog-QM fluorometer at excitation wavelength of 390 nm), compared in Figs. 3(h) and 3(g), respectively, show no measurable degradation of the liquid over the duration of the experiment, approximately 4 h at a 12-Hz repetition rate. Additional operation of more than 16 h shows no decrease in conversion efficiency.

It should be noted that our experimental setup is not optimized for maximal efficiency in any way: the cell length and diameter are chosen arbitrarily based on experience with water. None of the optics are coated, resulting in significant losses that can be easily reduced with properly antireflective parts, and proper wavelength separation can better be done with a dichroic mirror rather a prism. For MIR generation through DFG, pumping with the 1064-nm Nd:YAG fundamental would be preferable to reduce the quantum defect. However, under our experimental conditions we do not observe Raman shifting of the Nd:YAG fundamental because the absorption of EMIM DCA at the Stokes wavelength of 1390 nm is found to be too high. The fact that the liquid is not damaged even at high pumping energies suggests that the absorption at 1064 nm is low, since any significant absorption would result in optical damage.

While dye lasers can also operate in the yellow-orange range, the IL-based Raman converter has several advantages [56–58]: comparable efficiency can be achieved in a single-pass configuration without the need for a cavity for wavelength selection and linewidth narrowing. ILs do not exhibit triplet-state absorption at the signal wavelength

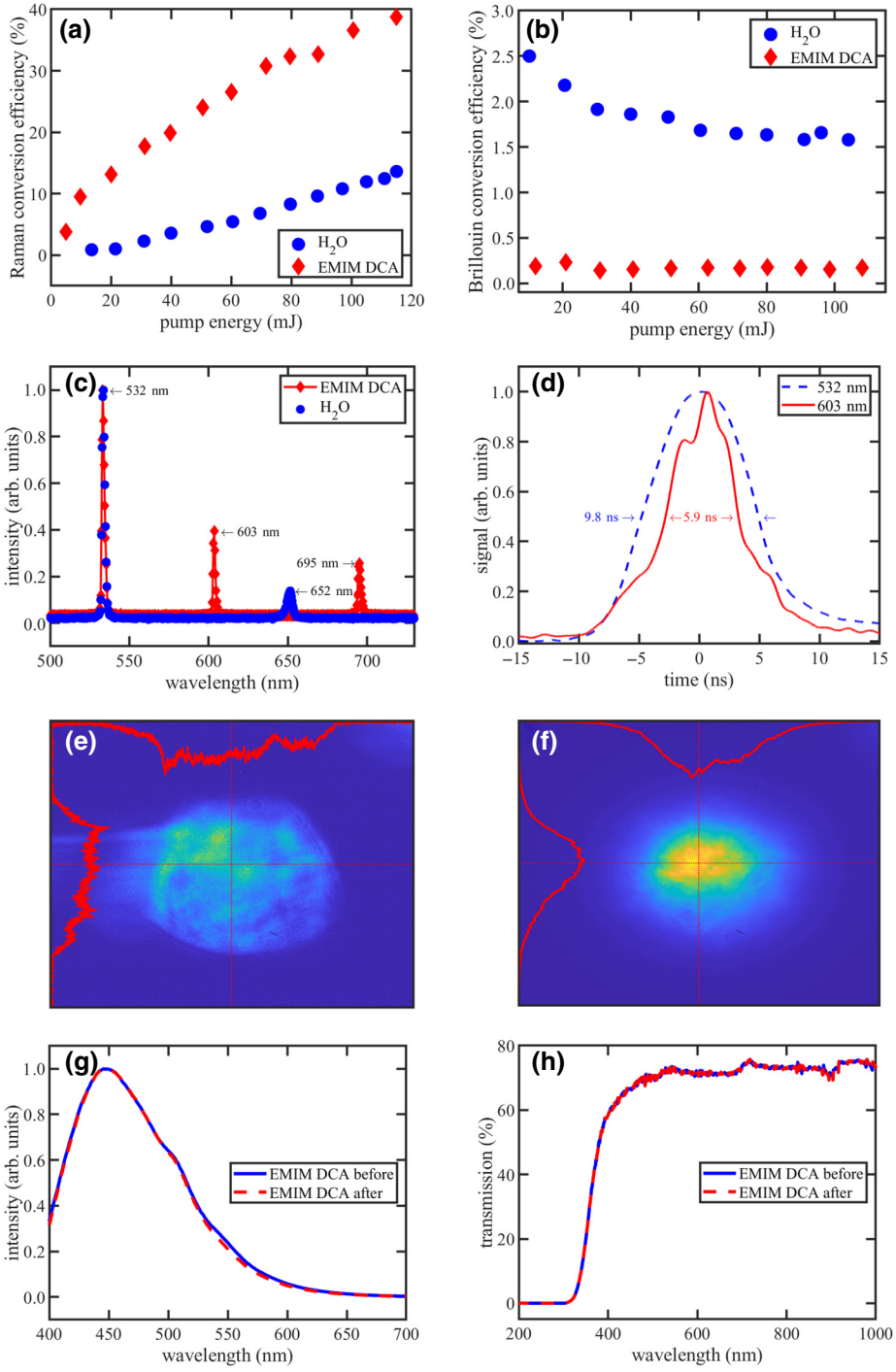

FIG. 3. Characterization of high-energy water and EMIM DCA Raman converters. (a) Conversion efficiency to the first Stokes order, defined as the ratio of first Stokes energy over pump energy and adjusted for optical losses in the optics except the liquid itself. EMIM DCA shows lower threshold energy and higher conversion efficiency than water. (b) Backward Brillouin scattering efficiency, defined as the ratio of excess backward signal (on top of reflection from the optics) over pump energy. The Brillouin scattering from EMIM DCA is negligible due to the high viscosity of the IL. (c) Optical spectrum after the converter. Note that the intensity of each peak depends on the orientation of the collection fiber tip and does not represent the actual intensity ratios. (d) Pump and Stokes temporal profiles (averaged over 300 shots) showing temporal shortening of the Stokes pulses. (e),(f) Profiles of the pump and Stokes beams, respectively, at the output of the converter at 25-mJ pump energy. The Stokes profile shows significant effective spatial cleaning of the multimode pump profile. Comparison of (g) fluorescence spectra and (h) UV-vis transmission spectra of a postexperiment EMIM DCA sample with an unused one shows no degradation of the liquid.

and are easier to handle compared with laser dyes, which are often toxic, carcinogenic, or corrosive. More generally, the nonresonant nature of SRS is insensitive to the wavelength pump source compared to in-band pumping of dye lasers, which can be useful for conversion from and to the NIR or when only fine detuning from the pump is needed. Like laser dyes, the liquid in an IL converter can be circulated for heat management. One drawback of SRS is that it cannot provide the on-the-fly tunability of dye lasers as the generated signal is set by the pump and the specific IL that are being used.

C. Tunability considerations

This demonstration is only one example of the wide variety of Raman shifting options possible with ILs. While we have a specific application in mind for targeting ILs that would provide a Stokes shift of around 2200 cm^{-1}, the tunability of ILs allows for a variety of possible Stokes shifts by selection of anions and cations with specific intense Raman bands. Figure 1(a) suggests that there are several non-nitrile ILs with strong Raman bands that could be used for shifting to other wavelengths. (It is important to remember that the spectra in Fig. 1(a) are arbitrarily scaled, so we are focusing on Raman bands that are more intense than the C—H stretching manifold between 2800 and 3200 cm^{-1}, which can be used as a rough reference for relative scaling.) For example, aryl groups generally have strong Raman bands in the region of 1000–1100 nm. In Fig. 1(a), 1-butylpyridinium bis(trifluoromethylsulfonyl)amide (BuPy NTf_2) shows a strong Raman band at 1029 cm^{-1} for the pyridinium ring, and aryl-functionalized 1-benzylpyridinium bis(trifluoromethylsulfonyl)amide (BzPy NTf_2) and 1-benzylpyridinium bis(fluorosulfonyl)amide (BzPy FSA) show strong Raman bands at 1020 and 1036 cm^{-1}, for the benzyl and pyridinium rings, respectively. Thus, pyridinium ILs or ILs containing benzyl functionalities could be used to shift a 532-nm laser beam to approximately 563 nm for the first Stokes shift and approximately 597 nm for the second one. Likewise, the NTf_2 anion, which is used in many ILs, has a strong Raman signal for the anion breathing mode [59] in the 740–750 cm^{-1} range, depending on the IL, that could shift 532 nm to about 554 and 578 nm for the first and second Stokes shifts, respectively.

To assess the Raman-shifting potential of ILs containing NTf_2 anions or aryl groups, we perform Raman-shifting experiments on 1-butyl-1-methylpyrrolidinium NTf_2 ($P_{1,4}$ NTf_2) and 1-butylpyridinium NTf_2 (BuPy NTf_2) in the same optical configuration used for EMIM DCA. The resulting spectra are shown in Fig. 4. Both ILs show a strong response, with $P_{1,4}$ NTf_2 displaying Stokes shifts up to fifth order and one anti-Stokes shift, with intervals of about 740 cm^{-1}. BuPy NTf_2 produces Stokes shifts up to fourth order and one anti-Stokes shift, with intervals of about 1033 cm^{-1}. Despite the presence of the NTf_2 anion in BuPy NTf_2, which contributes a strong Raman band at 740 cm^{-1}, the stronger pyridinium ring vibration at around 1033 cm^{-1} determines the observed Raman shifting. This has excellent implications for practical use since the NTf_2 anion is very commonly used in ILs for its inertness and its tendency to form ILs with desirable physical properties. This experiment shows that the NTf_2 anion can serve as a "silent partner" to provide desirable liquid properties when paired with an IL cation selected specifically for its Raman-shifting qualities.

Other ILs that we do not test could also be effective for Raman shifting. For example, the thiocyanate anion (SCN^-) in 1-butyl-3-methylimidazolium SCN has a

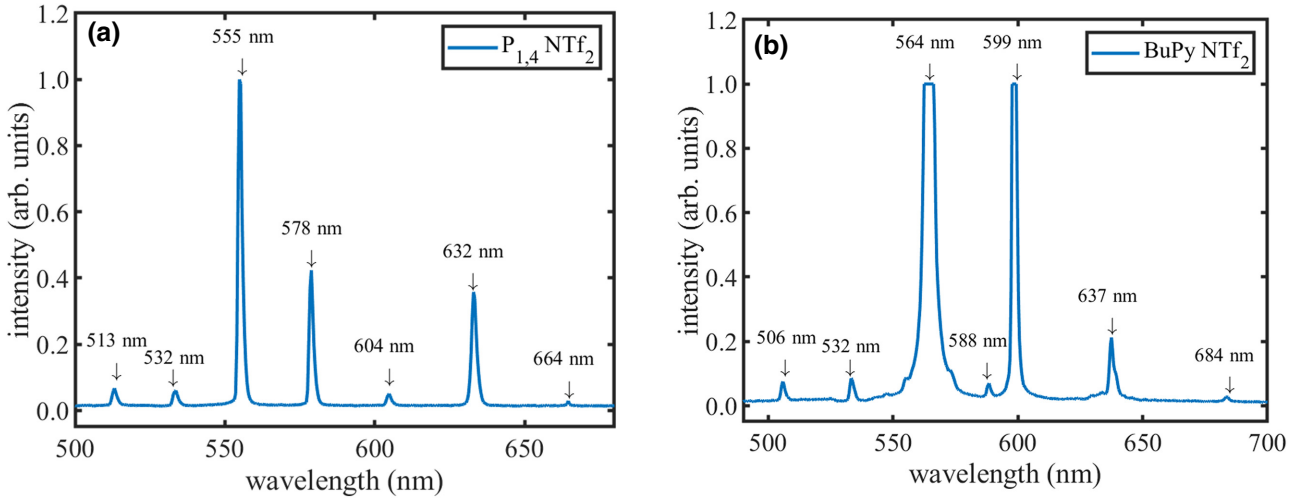

FIG. 4. Raman-shifting spectra of (a) $P_{1,4}$ NTf_2 and (b) BuPy NTf_2 with the pump wavelength attenuated by a 532-nm notch filter showing anti-Stokes and high-order Stokes conversions. Note that the intensity of each peak depends on the orientation of the collection fiber tip and does not represent the actual intensity ratios.

nitrile-centered Raman band [60] at 2040 cm^{-1} that could shift 532-nm laser light to around 597 and 680 nm for the first and second Stokes signals, respectively. Given that nitrate ions have proved effective in aqueous solution, nitrate ILs might work well. However, nitrate ILs with aprotic cations like EMIM tend to be solid at room temperature, and protic ILs with cations such as ethylammonium ($CH_3CH_2NH_3^+$) are relatively volatile because they can dissociate to the free amine (R-NH_2) and nitric acid when heated. In addition, the nitrate anion is a strong oxidant and IL cations contain fuel-like hydrocarbon groups, which is not a good combination in high-power laser applications. Since we demonstrate that aryl groups such as pyridinium cations effectively produce the same Raman shifts, the multiple complications of nitrate ILs would seem to render them unnecessary for Raman-shifting applications.

Physically, shift tunability can be thought of as an adjustment of the oscillator frequency $\omega_v = \sqrt{k/m}$ in a simple oscillator model by either adjusting the reduced mass (m, ions involved or isotopic substitution) or the effective force constant (k, type of chemical bond). Compared with solids, ILs allow greater freedom since they operate via molecular vibrational modes rather than collective phonons, and the desired vibrational modes can be designed into the molecules by the inclusion of specific structural motifs. This is readily applicable for the generation of high-energy laser radiation at wavelengths of interest where no good direct source is available, such as in our example with orange light, especially with shifts above the typical phonon energy in solids (greater than around 1300 cm^{-1}) or when a specific shift is needed. Another use is generation of MIR-LWIR by performing an additional step of frequency differentiation of the Raman-shifted light with the spent pump, which is our original motivation for this study. This also applies to shifting broadband ultrafast pulses that are stretched to more than a few picoseconds; for example, when a detuned, red-shifted probe is needed, a Raman-shifted portion can be generated from the main beam and can be used either in its chirped or fully compressed form. Thinking further ahead, the high refractive indices and low SBS of ILs make them interesting candidates to be incorporated into hollow-core fibers where their nonlinear properties could be exploited. Furthermore, if a suitable liquid can be found, it is intriguing to explore the possibility of generating MIR light directly in a single Raman shifting step by pumping with one of the emerging highly efficient short-wavelength infrared sources, such as thulium-doped yttrium lithium fluoride [61]. In the quantum mechanical picture, the Raman process can be understood as an absorption of the pump photon in a virtual state followed by stimulated emission of a Stokes photon. This intermediate short-lived virtual state is allowed due to the Heisenberg energy-time uncertainty principle. Typically, with a visible or NIR pump, this virtual state gains its short but finite lifetime from the probability tails of the excited electronic states with energies approximately comparable to UV photons. When using a longer wavelength pump, the virtual state gets further away from these excited electronic states and its lifetime gets shorter, leading to a decrease in cross section that scales as λ^{-4}. However, it would be interesting to test whether this scaling is valid at longer wavelengths or there is rather a change of trend in cross section when the virtual state nears the upper probability tails of molecular vibrational states and overtones, which are typically comparable to MIR photon energies.

III. CONCLUSION

This work demonstrates that ILs perform well as Raman wavelength converters. Our method allows efficient wavelength conversion of existing laser systems by simply passing the beam through a Raman conversion cell filled with a specifically tailored IL and with no sensitive alignment or phase-matching tuning. We provide examples of how to select an appropriate IL for a given conversion application by considering the chemical bonds that are responsible for the dominant Raman shift and optical absorption. As proof of principle, we demonstrate and characterize a high-energy IL-based single-pass Raman converter from 532 to 603 nm, and show the superior performance compared with liquid water. We show that different ILs can be selected to efficiently provide other wavelength conversions based on their chemical composition. More generally, we demonstrate the concept of using ILs as a nonlinear optical medium by showing that they can provide an engineerable framework to allow a wide range of wavelength shifts. We anticipate that this method could allow flexible and convenient generation of high-energy laser radiation in spectral regions that are useful for various scientific and medical applications but are challenging to attain with other techniques.

ACKNOWLEDGMENTS

This work was funded by BNL Laboratory Directed Research and Development Grants No. LDRD-001-21 and No. LDRD-18-026, and U.S. Department of Energy Contracts No. DE-SC0012704 and No. DE-AC52-07NA27344.

The authors declare no competing interests.

[1] R. W. Boyd, *Nonlinear Optics* (Elsevier, Cambridge, MA, 2003).

[2] E. L. Tanzi, J. R. Lupton, and T. S. Alster, Lasers in dermatology: Four decades of progress, J. Am. Acad. Dermatol. **49**, 1 (2003).

[3] M. Wanner, F. H. Sakamoto, M. M. Avram, H. H. Chan, M. Alam, Z. Tannous, and R. R. Anderson, Immediate

skin responses to laser and light treatments therapeutic endpoints: How to obtain efficacy, J. Am. Acad. Dermatol. **74**, 821 (2016).
[4] J. K. Chen, P. Ghasri, G. Aguilar, A. M. van Drooge, A. Wolkerstorfer, K. M. Kelly, and M. Heger, An overview of clinical and experimental treatment modalities for port wine stains, J. Am. Acad. Dermatol. **67**, 289 (2012).
[5] K. Inagaki, K. Ohkoshi, S. Ohde, G. A. Deshpande, N. Ebihara, and A. Murakami, Comparative efficacy of pure yellow (577-nm) and 810-nm subthreshold micropulse laser photocoagulation combined with yellow (561–577-nm) direct photocoagulation for diabetic macular edema, Jpn. J. Ophthalmol. **59**, 21 (2015).
[6] V. Kapoor, V. Karpov, C. Linton, F. v. Subach, V. v. Verkhusha, and W. G. Telford, Solid state yellow and orange lasers for flow cytometry, Cytometry, Part A. **73**, 570 (2008).
[7] C. V. Raman and K. S. Krishnan, A new type of secondary radiation, Nature **121**, 502 (1928).
[8] P. Cerný, H. Jelínková, P. G. Zverev, and T. T. Basiev, Solid state lasers with Raman frequency conversion, Prog. Quantum Electron. **28**, 113 (2004).
[9] A. Penzkofer, A. Laubereau, and W. Kaiser, High intensity Raman interactions, Prog. Quantum Electron. **6**, 55 (1979).
[10] K. Sentrayan, A. Michael, and V. Kushawaha, Intense backward Raman lasers in CH_4 and H_2, Appl. Opt. **32**, 930 (1993).
[11] Y. Ganot, S. Shrenkel, B. D. Barmashenko, and I. Bar, Enhanced stimulated Raman scattering in temperature controlled liquid water, App. Phys. Lett. **105**, 061107 (2014).
[12] N. Daher, X. Délen, F. Guichard, M. Hanna, and P. Georges, Raman wavelength conversion in a multipass cell, Opt. Lett. **46**, 3380 (2021).
[13] R. Casula, J.-P. Penttinen, M. Guina, A. J. Kemp, and J. E. Hastie, Cascaded crystalline Raman lasers for extended wavelength coverage: Continuous-wave, third-Stokes operation, Optica **5**, 1406 (2018).
[14] Y. F. Chen, D. Li, Y. M. Lee, C. C. Lee, H. Y. Huang, C. H. Tsou, and H. C. Liang, Highly efficient solid-state Raman yellow-orange lasers created by enhancing the cavity reflectivity, Opt. Lett. **46**, 797 (2021).
[15] N. Zhavoronkov, F. Noack, V. Petrov, V. P. Kalosha, and J. Herrmann, Chirped-pulse stimulated Raman scattering in barium nitrate with subsequent recompression, Opt. Lett. **26**, 47 (2001).
[16] F. B. Grigsby, P. Dong, and M. C. Downer, Chirped-pulse Raman amplification for two-color, high-intensity laser experiments, J. Opt. Soc. Am. B **25**, 346 (2008).
[17] H. Komine and E. A. Stappaerts, Efficient higher-Stokes-order Raman conversion in molecular gases, Opt. Lett. **4**, 398 (1979).
[18] A. I. Adamu, Y. Wang, R. Amezcua-Correa, O. Bang, and C. Markos, edited by L. Caspani, A. Tauke-Pedretti, F. Leo, and B. Yang in *Advanced Photonics Congress* (Optica Publishing Group, Washington DC, 2020).
[19] Y. Chen, Z. Wang, B. Gu, F. Yu, and Q. Lu, Achieving a 15 μm fiber gas Raman laser source with about 400 kW of peak power and a 63 GHz linewidth, Opt. Lett. **41**, 5118 (2016).
[20] F. Couny, F. Benabid, and P. S. Light, Subwatt Threshold cw Raman Fiber-Gas Laser Based on H_2-Filled Hollow-Core Photonic Crystal Fiber, Phys. Rev. Lett. **99**, 143903 (2007).
[21] P. A. Carpeggiani, G. Coccia, G. Fan, E. Kaksis, A. Pugžlys, A. Baltuška, R. Piccoli, Y.-G. Jeong, A. Rovere, R. Morandotti, *et al.*, Extreme Raman red shift: Ultrafast multimode nonlinear space-time dynamics, pulse compression, and broadly tunable frequency conversion, Optica **7**, 1349 (2020).
[22] F. Benabid, J. C. Knight, G. Antonopoulos, and P. J. Russel, Stimulated Raman scattering in hydrogen-filled hollow-core photonic crystal fiber, Science (1979) **298**, 399 (2002).
[23] B. Hafizi, J. P. Palastro, J. R. Peñano, T. G. Jones, L. A. Johnson, M. H. Helle, D. Kaganovich, Y. H. Chen, and A. B. Stamm, Stimulated Raman and Brillouin scattering, nonlinear focusing, thermal blooming, and optical breakdown of a laser beam propagating in water, J. Opt. Soc. Am. B **33**, 2062 (2016).
[24] Z. Hazan, Y. Ganot, and I. Bar, Suppression of self-induced thermal lensing in stimulated Raman scattering of liquids, J. Opt. Soc. Am. B **38**, 74 (2021).
[25] M. H. Helle, T. G. Jones, J. R. Peñano, D. Kaganovich, and A. Ting, Formation and propagation of meter-scale laser filaments in water, Appl. Phys. Lett. **103**, 121101 (2013).
[26] S. R. J. Brueck and H. Kildal, Efficient Raman frequency conversion in liquid nitrogen, IEEE J. Quantum Electron. **18**, 310 (1982).
[27] M. Armand, F. Endres, D. R. MacFarlane, H. Ohno, and B. Scrosati, Ionic-liquid materials for the electrochemical challenges of the future, Nat. Mater. **8**, 621 (2009).
[28] E. C. Welch, S. Ya. Tochitsky, J. J. Pigeon, and C. Joshi, Long-wave infrared picosecond parametric amplifier based on Raman shifter technology, Opt. Expr. **26**, 5154 (2018).
[29] R. D. Rogers and K. R. Seddon, Ionic liquids - solvents of the future?, Science (1979) **302**, 792 (2003).
[30] T. Welton, Room-temperature ionic liquids. Solvents for synthesis and catalysis, Chem. Rev. **99**, 2071 (1999).
[31] M. Galiński, A. Lewandowski, and I. Stepniak, Ionic liquids as electrolytes, Electrochim. Acta **51**, 5567 (2006).
[32] F. Zhou, Y. Liang, and W. Liu, Ionic liquid lubricants: Designed chemistry for engineering applications, Chem. Soc. Rev. **38**, 2590 (2009).
[33] A. Lainé, A. Niguès, L. Bocquet, and A. Siria, Nanotribology of Ionic Liquids: Transition to Yielding Response in Nanometric Confinement with Metallic Surfaces, Phys. Rev. X **10**, 011068 (2020).
[34] A. Schlaich, D. Jin, L. Bocquet, and B. Coasne, Electronic screening using a virtual Thomas–Fermi fluid for predicting wetting and phase transitions of ionic liquids at metal surfaces, Nat. Mater. **21**, 237 (2022).
[35] M. Watanabe, M. L. Thomas, S. Zhang, K. Ueno, T. Yasuda, and K. Dokko, Application of ionic liquids to energy storage and conversion materials and devices, Chem. Rev. **117**, 7190 (2017).
[36] N. v. Plechkova and K. R. Seddon, Applications of ionic liquids in the chemical industry, Chem. Soc. Rev. **37**, 123 (2008).
[37] J. F. Wishart, Energy applications of ionic liquids, Energy Environ. Sci. **2**, 956 (2009).

[38] J. Shi, Y. Tang, H. Wei, L. Zhang, D. Zhang, J. Shi, W. Gong, X. He, K. Yang, and D. Liu, Temperature dependence of threshold and gain coefficient of stimulated Brillouin scattering in water, Appl. Phys. B **108**, 717 (2012).

[39] R. W. Boyd, K. Rzyzewski, and P. Narum, Noise initiation of stimulated Brillouin scattering, Phys. Rev. A **42**, 5514 (1990).

[40] J. Shi, J. Xu, Y. Guo, N. Luo, S. Li, and X. He, Dependence of Stimulated Brillouin Scattering in Water on Temperature, Pressure, and Attenuation Coefficient, Phys. Rev. Appl. **15**, 054024 (2021).

[41] M. N. Polyanskiy, I. v. Pogorelsky, M. Babzien, R. Kupfer, N. Vafaei-Najafabadi, and M. A. Palmer, High-peak-power long-wave infrared lasers with CO_2 amplifiers, Photonics **8**, 101 (2021).

[42] M. N. Polyanskiy, I. v Pogorelsky, and V. Yakimenko, Picosecond pulse amplification in isotopic CO_2 active medium, Opt. Expr. **19**, 7717 (2011).

[43] M. N. Polyanskiy, I. v. Pogorelsky, M. Babzien, and M. A. Palmer, Demonstration of a 2 ps, 5 TW peak power, long-wave infrared laser based on chirped-pulse amplification with mixed-isotope CO_2 amplifiers, OSA Continuum **3**, 459 (2020).

[44] D. Tovey, S. Ya. Tochitsky, J. J. Pigeon, G. J. Louwrens, M. N. Polyanskiy, I. Ben-Zvi, and C. Joshi, Multi-atmosphere picosecond CO_2 amplifier optically pumped at 43 μm, Appl. Opt. **58**, 5756 (2019).

[45] V. M. Gordienko and V. T. Platonenko, Regenerative amplification of picosecond 10-μm pulses in a high-pressure optically pumped CO_2 laser, Quantum Electron. **40**, 1118 (2011).

[46] I. A. Shkrob, T. W. Marin, S. D. Chemerisov, and J. F. Wishart, Radiation induced redox reactions and fragmentation of constituent ions in ionic liquids. 1. Anions, J. Phys. Chem. B **115**, 3872 (2011).

[47] H. Shirota, H. Matsuzaki, S. Ramati, and J. F. Wishart, Effects of aromaticity in cations and their functional groups on the low-frequency spectra and physical properties of ionic liquids, J. Phys. Chem. B **119**, 9173 (2015).

[48] S. N. Suarez, A. Rúa, D. Cuffari, K. Pilar, J. L. Hatcher, S. Ramati, and J. F. Wishart, Do TFSA anions slither? Pressure exposes the role of TFSA conformational exchange in self-diffusion, J. Phys. Chem. B **119**, 14756 (2015).

[49] Z. Ye, C. Liu, B. Tu, K. Wang, Q. Gao, C. Tang, and Z. Cai, Kilowatt-level direct-'refractive index matching liquid'-cooled Nd :YLF thin disk laser resonator, Opt. Express **24**, 1758 (2016).

[50] J. M. P. Franca, M. J. v. Lourenco, M. Sohel Murshed, A. A. H. Padua, and C. A. Nieto de Castro, Thermal conductivity of ionic liquids and ionanofluids and their feasibility as heat transfer fluids, Ind. Eng. Chem. Res. **57**, 6516 (2018).

[51] J. M. P. França, F. Reis, S. I. C. Vieira, M. J. V. Lourenço, F. J. V. Santos, C. A. Nieto De Castro, and A. A. H. Pádua, Thermophysical properties of ionic liquid dicyanamide (DCA) nanosystems dedicated to the memory of the late Professor Manuel Ribeiro da Silva, J. Chem. Thermodyn. **79**, 248 (2014).

[52] J. M. P. França, C. A. Nieto De Castro, M. M. Lopes, and V. M. B. Nunes, Influence of thermophysical properties of ionic liquids in chemical process design, J. Chem. Eng. Data **54**, 2569 (2009).

[53] C. Schreiner, S. Zugmann, R. Hartl, and H. J. Gores, Fractional Walden rule for ionic liquids: Examples from recent measurements and a critique of the so-called ideal KCl line for the Walden plot, J. Chem. Eng. Data **55**, 1784 (2010).

[54] I. A. Shkrob, T. W. Marin, S. D. Chemerisov, J. L. Hatcher, and J. F. Wishart, Radiation induced redox reactions and fragmentation of constituent ions in ionic liquids. 2. Imidazolium cations, J. Phys. Chem. B **115**, 3889 (2011).

[55] P. Navarro, M. Larriba, E. Rojo, J. García, and F. Rodríguez, Thermal properties of cyano-based ionic liquids, J. Chem. Eng. Data **58**, 2187 (2013).

[56] T. G. Pavlopoulos, Scaling of dye lasers with improved laser dyes, Prog. Quantum. Electron. **26**, 193 (2002).

[57] C. v Shank, Physics of dye lasers, Rev. Mod. Phys. **47**, 649 (1975).

[58] F. J. Duarte, Organic dye lasers: Brief history and recent developments, Opt. Photonics News **14**, 20 (2003).

[59] L. F. O. Faria, M. M. Nobrega, M. L. A. Temperini, and M. C. C. Ribeiro, Ionic liquids based on the bis(trifluoromethylsulfonyl)imide anion for high-pressure Raman spectroscopy measurements, J. Raman Spectrosc. **44**, 481 (2013).

[60] C. Y. Peñalber, Z. Grenoble, G. A. Baker, and S. Baldelli, Surface characterization of imidazolium-based ionic liquids with cyano-functionalized anions at the gas-liquid interface using sum frequency generation spectroscopy, Phys. Chem. Chem. Phys. **14**, 5122 (2012).

[61] I. Tamer, B. A. Reagan, T. Galvin, J. Galbraith, E. Sistrunk, A. Church, G. Huete, H. Neurath, and T. Spinka, Demonstration of a compact, multi-joule, diode-pumped Tm:YLF laser, Opt. Lett. **46**, 5096 (2021).